Published in final edited form as:
Curr Biol. 2009 October 13; 19(19): 1599–1607. doi:10.1016/j.cub.2009.08.045.

The CIL-1 phosphoinositide 5-phosphatase regulates ciliary localization of the TRP polycystins and sperm function in *C. elegans*

Young-Kyung Bae[1,#], **Eunsoo Kim**[2], **Steven W. L'Hernault**[3], and **Maureen M. Barr**[1]

[1]Department of Genetics, Rutgers University, the State University of New Jersey, Piscataway, NJ 08854, USA

[2]Department of Biochemistry and Molecular Biology, Dalhousie University, 5850 College St., Halifax NS B3H 1X5 Canada

[3]Department of Biology, Emory University, Atlanta GA 30332

Summary

Background—*C. elegans* male sexual behaviors include chemotaxis and response to hermaphrodites, backing/turning, vulva location, spicule insertion and sperm transfer, culminating in cross fertilization of hermaphrodite oocytes with male sperm. The LOV-1 and PKD-2 transient receptor potential polycystin (TRPP) complex localizes to ciliated endings of *C. elegans* male-specific sensory neurons and mediates several aspects of male mating behavior. TRPP complex ciliary localization and sensory function is evolutionarily conserved. A genetic screen for *C. elegans* mutants with PKD-2 ciliary localization (Cil) defects led to the isolation of a mutation in the *cil-1* gene.

Results—Here, we report that a phosphoinositide (PI) 5-phosphatase CIL-1 regulates TRPP complex ciliary receptor localization and sperm activation. *cil-1* does not regulate the localization of other ciliary proteins, including intraflagellar transport (IFT) components, sensory receptors, or other TRP channels in different cell types. Rather, *cil-1* specifically controls TRPP complex trafficking in male-specific sensory neurons and does so in a cell autonomous fashion. In these cells, *cil-1* is required for normal PI(3)P distribution, indicating that a balance between PI(3,5)P2 and PI (3)P is important for TRPP localization. *cil-1* mutants are infertile due to sperm activation and motility defects. In sperm, the CIL-1 5-phosphatase and a wortmannin sensitive PI 3-kinase act antagonistically to regulate the conversion of sessile spermatids into motile spermatozoa, implicating PI(3,4,5)P3 signaling in nematode sperm activation.

Conclusion—Our studies identify the CIL-1 5-phosphatase as key regulator of PI metabolism in cell types that are important in several aspects of male reproductive biology.

Address correspondence to Dr. Maureen M. Barr, Department of Genetics, Rutgers University, 145 Bevier Road, Piscataway, NJ 08854. Tel: 732-445-1639. Fax: 732-445-1147. barr@biology.rutgers.edu.
[#]current address: Department of Biology, The California Institute of Technology, Pasadena, CA

Experimental Procedures: Refer to Supplement

Introduction

Phosphoinositides (PIs) and their phosphatases and kinases play pivotal roles in receptor trafficking as well as in membrane organelle biogenesis/transport, endocytosis, cytoskeleton dynamics, signal transduction, cell motility, and channel activity modulation [1,2]. Many sensory receptors localize to ciliary membrane, which serve as cellular antennae and function in development, signaling, and physiology. Whether PIs and PI-generating enzymes regulate ciliary receptor trafficking is unknown.

The nematode *Caenorhabditis elegans* is a powerful model to study molecular mechanisms required for ciliary receptor trafficking. The *C. elegans* transient receptor potential polycystin (TRPP) complex proteins LOV-1 (TRPP1) and PKD-2 (TRPP2) localize to sensory cilia [3, 4]. Autosomal dominant polycystic kidney disease (ADPKD) is caused by mutations in the TRPP1 and TRPP2 genes [5]. Since the discovery of LOV-1 and PKD-2 in cilia of *C. elegans* male-specific sensory neurons, TRPPs have been found in primary cilia or flagella in organisms ranging from alga to man, hinting at an evolutionarily conserved mechanism regulating TRPP ciliary localization (reviewed in [6]).

In diverse species, TRPP family proteins serve reproductive functions [7-12]. *C. elegans* LOV-1 and PKD-2 function in male mating behaviors. *pkd-2* appears to be expressed solely in the male nervous system and not sperm, as judged by antibody staining [4]. In contrast to mammalian and *Drosophila* sperm, nematode sperm are not flagellated and do not possess an actin/tubulin cytoskeleton (reviewed in [13]). Instead, each sperm extends a single pseudopod enriched with major sperm protein (MSP). MSP is used to assemble a filamentous network required for amoeboid motility and fertilization. Screens have identified genes required for spermatogenesis, hermaphrodite sperm activation, and sperm function. Signaling pathways involved in sperm activation in both males and hermaphrodites are not known.

PKD-2 ciliary localization requires vesicular trafficking and utilizes both general and cell-type specific factors [14]. General factors include the clathrin coated vesicle adaptor protein-1 (AP-1) UNC-101 and the intraflagellar transport (IFT) machinery. Cell-type specific PKD-2 localization factors include LOV-1 and STAM-Hrs (Signal-transducing adaptor molecule and hepatocyte growth factor regulated tyrosine kinase substrate) complex [14,15]. We performed a genetic screen for *C. elegans* mutants with PKD-2 ciliary localization (Cil) defects [16]. Here, we identify CIL-1, a PI 5-phosphatase that regulates TRPP complex localization. *cil-1* is also a positive regulator of sperm activation and motility. Using genetically encoded PI-indicators and pharmacological approaches, we determine that CIL-1 hydrolyses PI(3,5)P2 and PI(3,4,5) P3 in male-specific sensory neurons and sperm, respectively. We conclude that CIL-1 acts in multiple tissues that are important for male reproductive biology, thereby controlling diverse cellular processes as an in vivo PI-metabolizing enzyme.

Results

cil-1 is required for LOV-1 and PKD-2 localization

In wild type (WT), PKD-2::GFP localizes to cell bodies and ciliary endings of 21 male-specific neurons in the head (cephalic CEMs) and tail (ray RnBs and hook HOB) ([14], Figure 1A-D). In *my15* mutants, PKD-2::GFP is distributed throughout these male-specific neurons including dendrites, axons, cell bodies, and cilia (Figure 1E-F). *cil-1* is not required for neuronal cell fate or development of *pkd-2* expressing neurons as judged by reporters including transcriptional and soluble P*pkd-2*::GFP, OSM-6::GFP (data not shown), P*pkd-2*:SNB-1:GFP (Supplemental Figure 1, SF1), and fluorescent protein tagged PI-markers (SF4). P*pkd-2*::GFP and endogenous *pkd-2* mRNA levels are unaltered in *my15* animals as judged by qRT-PCR (data not shown), indicating that *my15* may affect PKD-2 protein expression or stability, but not gene expression.

In WT and *my15* dendrites, small PKD-2::GFP particles move bidirectionally (Supplemental Movies 1 and 2), indicating that a pool of PKD-2::GFP is properly trafficked in *my15* dendrites. Moreover, PKD-2::GFP distribution in the *my15* ciliary region appears normal, despite abnormally increased dendritic and axonal distributions (Figure 1E-F, [16]).

We examined the distribution of additional GFP-tagged ciliary proteins, including functional LOV-1::GFP ([15], SF1A-D), a TRP-vanilloid OSM-9, a G-protein coupled receptor (GPCR) ODR-10, an IFT B-complex polypeptide OSM-6, and IFT modulator BBS-5. Only LOV-1::GFP is abnormally distributed to dendritic and axonal processes in *my15* sensory neurons (SF1C-D). We also examined the localization of the presynaptic marker synaptobrevin P*pkd-2*::SNB-1::GFP [17]. In WT and *my15* males, SNB-1::GFP labels presynaptic puncta along axonal processes (SF1E-F), indicating that *cil-1* does not grossly affect axonal targeting. *my15* mutants are normal in lipophilic DiI dye-filling of ciliated sensory neurons, chemotaxis to diacetyl, dauer formation, and osmotic avoidance (data not shown). We conclude that *cil-1* is specifically required for localization of the TRPP complex, but not for general receptor trafficking, ciliogenesis, neuronal polarization, or sensation.

lov-1, *pkd-2*, and a subset of Cil mutants, are response and location of vulva (Lov) defective during male mating [3,4,16]. *my15* males exhibit normal response and vulva location behaviors (SF1G, [16]), which may be explained by the presence of PKD-2::GFP in cilia. *cil-1* double or triple homozygous or trans heterozygous mutants with *pkd-2* and *lov-1* did not alter male mating efficiency, indicating that *cil-1* is not a genetic modifier of the *C. elegans* TRPP genes (data not shown). Although mating behaviors appear normal, *my15* males are largely infertile and produce few offspring due to a sperm (Spe) defect, which will be discussed later.

cil-1 acts between *lov-1* and *stam-1* in RnB ray neurons

We previously showed that TRPP complex formation is important for trafficking [14]. In a *lov-1* mutant, PKD-2::GFP forms aggregates in cell bodies and localizes to cilia at a reduced level (Figure 1G-H). In *lov-1; cil-1* CEM neurons (Fig 1I), the PKD-2::GFP localization phenotype is additive: bright aggregates in the cell bodies (*lov-1* phenotype; white arrows) and mislocalization to the dendrites and axons (*cil-l* phenotype), albeit at reduced levels (red arrows). In *lov-1; cil-1* RnB neurons (Figure 1J), the PKD-2::GFP localization phenotype resembles that of *lov-1* but not *cil-1*: aggregates in the cell body and absence from dendritic and ciliary compartments. This strict requirement of *lov-1* in RnB as compared to CEM neurons has been previously shown for PKD-2 ciliary targeting [14]. The basis of this cell type specificity is unknown, but may be due to differences in protein trafficking mechanisms or structural differences between CEM and RnB neurons.

PKD-2 ciliary abundance is tightly controlled. STAM and Hrs mediate PKD-2 and LOV-1 downregulation via transport from early endosomes to endosomal sorting complexes (ESCRT) [15]. Reducing *stam-1* or *hgrs-1* function results in PKD-2::GFP and LOV-1::GFP accumulation at the ciliary base (Figure 1K-L, [15]). In CEM neurons of a *stam-1*(*ok406*)*; cil-1 (my15)* double mutant (Figure 1M), the PKD-2::GFP localization phenotype is additive. In *stam-1; cil-1* RnB neurons (Figure 1N), PKD-2::GFP is distributed evenly throughout, similar to *cil-1* single mutants. We conclude that, in RnB neurons, *cil-1* acts after *lov-1* but before *stam-1*. In CEMs, the *lov-1; cil-1* and *cil-1; stam-1* phenotype is complex, making it difficult to place *lov-1*, *cil-1*, and *stam-1* in a linear or parallel pathway.

cil-1 encodes a phosphoinositide 5-phosphatase that acts cell autonomously

The smallest rescuing genomic fragment for both the Cil and Spe phenotypes (8160K-1, Figure 2A-B) contains two genes, C50C3.7 and *bath-42* in the operon CEOP3484. The *bath-42 (tm2360)* deletion mutant is nonCil and nonSpe (data not shown). A construct containing 2.2kb

5′ UTR of the *bath-42* and the C50C3.7 genomic region including the 3′UTR rescues both Cil and Spe phenotypes of *my15* (PCR-SOEed C50C3.7, Figure 2A-B). Sequencing analysis of *my15* genomic DNA identified a G→A transition that converts Trp^{301} (TGG) to a stop codon (TAG) in the 5^{th} exon of C50C3.7 (Figure 2A). From both WT and *my15* cDNA pools, RT (reverse transcriptase)-PCR identified two *cil-1* cDNAs (long C50C3.7a and short C50C3.7b). The short form (C50C3.7b) is generated by alternative splicing within the 3^{rd} intron, introducing a stop codon at 124^{th} amino acid before the *my15* induced lesion. P*pkd-2*::CIL-1a (C50C3.7a)::tdTomato fully rescues the *cil-1(my15)* Cil but not Spe phenotype (Figure 2A, B), which is not surprising given that *pkd-2* is not expressed in sperm. In contrast, expression of C50C3.7a using an intestinal promoter fails to rescue the Cil phenotype (data not shown). We did not attempt to rescue the *cil-1(my15)* Spe phenotype using cell-type specific promoters as transgenes are often silenced in the germline. We conclude that C50C3.7 is the gene mutated in *cil-1(my15)* animals and that CIL-1 acts autonomously in male-specific neurons to control TRPP localization.

cil-1 encodes a phosphoinositide (PI) 5-phosphatase (referred as 5-phosphatase), which removes the D-5 phosphate from the inositol ring of membrane associated PI or soluble inositol phosphates. The 5-phosphatase family comprises ten mammalian, four yeast, and five *C. elegans* enzymes. Phylogenetic analysis of the 5-phosphatase catalytic domain and/or of the presence or absence of adjacent domains reveals that CIL-1 is closely associated with two mammalian 5-phosphatases: SKIP (skeletal muscle and kidney enriched inositol phosphatase) and PIPP (proline rich inositol polyphosphate phosphatase). CIL-1, SKIP, and PIPP belong to SKICH (SKIP carboxyl homology) subfamily, which contains a C-terminal SKICH-like domain (SF2A, D) and mediates protein localization [18].

The *C. elegans* genome encodes five 5-phosphatase genes: *ipp-5*, *unc-26*, *ocrl-1*, *cil-1*/C50C3.7, and T25B9.10. *ipp-5* (Type I) negatively regulates ovulation by inhibiting inositol 1,4,5-triphosphate (IP3) signaling in the spermatheca [19]. IP3 signaling also regulates mating behavior steps of turning, spicule insertion, and sperm transfer [20]. *unc-26* (synaptojanin) is required for synaptic vesicle endocytosis and recycling, with mutants exhibiting uncoordinated movements [21]. Neither *ipp-5* nor *unc-26* mutant is Cil or Spe defective, and *cil-1(my15)* mutants are normal in ovulation, locomotion, male turning, spicule insertion, and sperm transfer, ruling out possible overlapping functions (data not shown).

CIL-1 contains two conserved 5-phosphatase motifs in its catalytic domain (SF2B). We introduced a missense mutation in a known critical residue of 5-phosphatase motif ($CIL\text{-}1^{N175A}$, SF2B, red arrowhead). P*pkd-2*::$CIL\text{-}1^{N175A}$::tdTomato failed to rescue the *my15* Cil phenotype, indicating that phosphatase catalytic activity is required for CIL-1 function.

In male neurons, the rescuing P*pkd-2*::CIL-1::tdTomato is distributed in cilia, dendrites, axons, cell bodies with occasional small puncta, and weakly in nuclei (SF3D), and is often visible as bright dots at ciliary bases of ray neurons (SF3E), suggesting CIL-1 function in ciliary regions. In the intestine, P*vha-6*::CIL-1::GFP localizes to cytoplasmic reticular structures (SF3F).

CIL-1 regulates PI(3,4)P2/PI(3,4,5)P3 and PI(3)P but not PI(4,5)P2 levels

Seven PI species are generated by the reversible phosphorylation and dephosphorylation. To determine what PI species are CIL-1 substrates, we expressed genetically encoded biosensors to detect changes in specific PI lipid concentrations in male-specific sensory neurons and the intestine. We observed obvious differences in PI(3)P Hrs(2×FYVE) and PI(3,4)P2/PI(3,4,5)P3 AKT(PH), but not PI(4,5)P2 (PH domain of PLC-delta) markers between WT and *cil-1 (my15)* animals. In the WT intestine, PI(3)P is primarily found in tubulovesicular structures without any plasma membrane (PM) enrichment, similar to the CIL-1 distribution pattern

(compare Figure 3A with SF3F). In the *cil-1* intestine, PI(3)P is severely disrupted, with a diffuse pattern in the cytoplasm (Figure 3D). In WT intestine, PI(3,4)P2/PI(3,4,5)P3, is found in tubulovesicular structures and enriched at the PM (Figure 3B, arrowheads and arrow). In *cil-1(my15)* mutants, the PI(3,4)P2/PI(3,4,5)P3 marker labels no distinct structure, appearing diffuse in the cytoplasm with no PM enrichment. A similar pattern has been reported in *C. elegans let-512/vps-34* PI 3-kinase mutants, in which PI(3)P generation is reduced [22]. In both WT and *cil-1(my15)* intestine, PI(4,5)P2 is enriched at the apical PM lining the intestinal lumen as well as basolateral PM (Figure 3C-F). These data indicate that CIL-1 displays in vivo phosphatase activity towards PI(3,4,5)P3 and PI(3,5)P2 in the intestine.

In male-specific sensory neurons, we observe differences in PI(3)P distribution (Figure 3G-H), but not PI(3,4)P2/PI(3,4,5)P3 or PI(4,5)P2 markers in *cil-1(my15)* males (SF4). In WT neurons, the PI(3)P marker is enriched in nuclei, small puncta in the cell bodies, but rarely in dendritic and ciliary regions (Figure 3G, G′), with only 1/13 animals displaying detectable expression in dendrites and cilia. In *cil-1(my15)*, the PI(3)P marker decorates dendritic processes and cilia (16/27 animals) in addition to the enrichment in the nuclei and cell bodies (Figure 3H, 4H′). The PI(3)P marker is distinctly bright at *cil-1(my15)* ciliary bases (Figure 3H inset), hinting that loss of CIL-1 perturbs PI(3)P distribution in this region. These data suggest that CIL-1 displays a tissue-specific substrate preference towards PI(3,5)P2 in male sensory neurons.

Since PI(3)P localizes to early endosomes, we examined early endosomal protein distribution. RAB-5 is an early endosomal protein that recruits and activates PI(3)P generating PI 3-kinases [23]. STAM-1 colocalizes with RAB-5 in *C. elegans* male specific sensory neurons and promotes polycystin trafficking from early endosomes to the ESCRT complex [15]. In WT and *cil-1(my15)* animals, RAB-5 and STAM-1 localize to small puncta in the cell bodies, axons, and dendrites (SF4G-J), indicating that *cil-1* does not modify the overall organization of early endosomes.

cil-1 mutants are sperm defective

cil-1(my15) hermaphrodites exhibit a drastic reduction in brood size (4.85% of WT) (SF5A), which is due to a spermatogenesis defect (Spe) based on the following observations. (1) a *my15* hermaphrodite lays 200-300 unfertilized eggs, which is comparable to the number of WT fertilized eggs (SF5A), (2) *my15* male germline architecture and early stages of spermatogenesis (data not shown), hermaphrodite oocyte maturation, and ovulation appear normal (Suppl. Figure 4D-E), (3) *my15* hermaphrodites contain endomitotic cells without eggshells in the uterus (SF5F-G), (4) the *my15* fertility defect is completely rescued when mated with WT males (SF5B), (5) *my15* males fail to sire cross progeny without overt behavioral defects in mating behaviors (SF5C and SF1G). We conclude that *cil-1* is required for sperm function in both hermaphrodites and males.

A Spe phenotype may arise from developmental defects in spermatogenesis, sperm activation (spermiogenesis), sperm motility, or sperm-egg interactions. *my15* male gonads have normal DAPI staining patterns for each meiotic stage in the gonad and normal number of spermatids (inactive 1N sperm) (data not shown). Thus, *cil-1* is not required for early spermatogenesis up to spermatid production. Defective sperm-egg interactions are the basis of Spe phenotypes in *spe-9*, *spe-38*, *trp-3/spe-41*, and *spe-42* (Figure 4A) (reviewed by [13]). In these Spe mutants, male-derived sperm normally develop, activate, crawl, and compete with endogenous hermaphroditic sperm, but cannot fertilize an oocyte. However, *my15* male-derived sperm do not compete with endogenous hermaphrodite-derived sperm, as reflected by a large number of self-progeny and extremely low mating efficiency (ME) (1.9%, SF5C). ME of WT males is higher with *my15* hermaphrodites (~95%) than control hermaphrodites (58%) (SF5C), illustrating that *my15* endogenous sperm are nearly incapable of competing with WT male-

derived sperm. Hence *cil-1* acts in events between spermatid production and sperm-egg interactions.

cil-1 is required for sperm activation and motility

During sperm activation, a round spermatid develops into a motile spermatozoon with a pseudopod (Figure 4A). This process can be mimicked in vitro by chemical activators such as the ionophore monensin or Pronase (reviewed by [13]). Within 15 minutes of Pronase application, the majority of WT male spermatids (63.4%, n=347) extend pseudopods (Figure 4B-B′) and the average length of spermatozoa is 8.13 ± 1.11 um (±stdev, n=95) (Figure 4B′). In contrast, only 47.8% (n=128) of *my15* male spermatids develop pseudopods after Pronase activation (Figure 4C-C′) with a significantly shorter spermatozoa length (6.37 ± 0.61um (n=112), p =1.09E-28, Figure 4C′). The diameter of *my15* spermatids is also slightly smaller (6.22 ± 0.54 um, n=136) than WT (6.73 ± 0.65 um, n=110, p=8.08E-07). We also observe in vivo sperm activation defects in *my15* hermaphrodites. 83.3% of WT spermatozoa possess pseudopods (n=36, Figure 4B″) whereas only 8.3% do in *my15* mutants (n=72, Figure 4C″). When present, *my15* pseudopods are significantly shorter (average length of longest axes of sperm; 4.32 ± 0.38 um, n=6) than WT (5.43 ± 0.62 um, n=37, p=1.14E-4). Thus, *cil-1* positively regulates sperm activation in vitro and in vivo.

To measure *my15* sperm motility, we performed a time-lapse sperm tracking assay. WT male sperm crawl from the uterus to the spermatheca over time, with the majority localizing at the spermatheca in 16 hours (Figure 4D). In contrast, *my15* sperm are not observed in the spermatheca at 16 hours despite being present at 4 hours (Figure 4D). These data suggest that *my15* sperm display reduced motility and, consequently, are not retained in the hermaphrodite spermatheca. After in vitro chemical activation with monensin, WT sperm crawl at the rate of 0.33 ± 0.04 μm/sec (n=7) on glass slides (Suppl. Movie 3) whereas isolated *my15* sperm are immotile (Suppl. Movie 4).

Sperm activation involves fusion of membranous organelles (MOs) to the PM, exocytosis, and pseudopod extension (reviewed by [13]). To examine MOs, we used the MO specific monoclonal antibody 1CB4 [24] and the lipophilic dye FM1-43 [25]. In WT, the majority of MOs are found at the cell periphery of round spermatids (Figure 4H). After activation, MOs are excluded from the pseudopod (Figure 4H′). In *my15* sperm, 1CB4 staining for MO morphology and localization before and after activation appears WT (Figure 4I, I′). In both WT and *my15*, FM1-43 labels the PM of the round spermatids (Figure 4F-G) and, after activation, concentrates at the site membrane fusion on the spermatozoon cell body (Figure 4F′, G′, arrowheads). *cil-1* is not essential for MO morphology, localization, or fusion.

The ultrastructure of *my15* sperm is largely unaffected as determined by transmission electron microscopy (TEM). The early stages of spermatogenesis in WT and *my15* appear very similar (data not shown). Occasionally, dissected males will produce spontaneously activated spermatozoa, and we examined such cells in both WT and *my15* (Figure 4E, E′). In both cases, a pseudopod is extended and separated from the cell body by laminar membranes. MOs successfully fuse with the PM in *my15*, consistent with immunostaining and MO fusion assay (Figure 4G′, I′).

cil-1 may regulate membrane receptor localization in sperm. TRP-3/SPE-41 acts in sperm, translocates from MOs to the PM upon activation, and is required for fertilization [26]. In WT and *my15* spermatids, anti-TRP-3 labels cytoplasmic puncta partially overlapping with MOs (Figure 4H, I). In WT and *my15* spermatozoa, TRP-3 is detected ubiquitously on the PM of the pseudopod and cell body (Figure 5H″, I″). *cil-1* is not required for TRP-3/TRPC translocation to the PM.

CIL-1 and PI 3-Kinase activity antagonistically regulate sperm activation

Since PI biosensors show that CIL-1 hydrolyzes PI(3,4,5)P3 and PI(3,5)P2, we asked whether 3-kinase activity antagonizes CIL-1 5-phosphatase function. We applied 1nM, 10nM, and 100nM wortmannin, a pharmacological inhibitor of PI 3-kinases that produce PI(3,4,5)P3 from PI(4,5)P2 [27], to WT and *my15* spermatids. At all concentrations tested, wortmannin acts as an in vitro activator of WT but not *my15* spermatids, with 100nM being the most effective (compare Figure 4B‴ with 4C‴). The low dose (1nM) of wortmannin suggests specificity, and indicates PI 3-kinase activity and *cil-1* act antagonistically in sperm activation (Figure 5C, D).

Discussion

The PI 5-phosphatase CIL-1 mediates multiple aspects of *C. elegans* male reproductive biology (Figure 5). In male neurons, *cil-1* acts cell autonomously to control LOV-1 and PKD-2 localization but not function. Our data supports a model whereby *cil-1* acts in early steps in TRPP complex downregulation by regulating PI(3)P distribution but not RAB-5 and STAM localization (Figure 5A, B). In sperm, *cil-1* positively regulates sperm activation and motility without affecting major membrane trafficking events. The 3-kinase inhibitor wortmannin is a potent sperm activator, which indicates that PI(3,4,5)P3 is a major CIL-1 substrate in sperm. We propose that one of the three 3-kinase encoded in the *C. elegans* genome (VPS-34, AGE-1, or F39B1.1) acts antagonistically to CIL-1 in a sperm activation pathway (Figure 5C, D).

cil-1 may be required for cellular polarity as distinct PI enrichment is a hallmark of polarized plasma membrane domains [28,29]. However, *cil-1* mutants properly localize several other ciliary and presynaptic markers (SF1), and exhibit normal sensory behaviors, reflecting properly polarized and functional neurons. Alternatively, *cil-1* may modulate the activity of the TRPP complex. PI(4,5)P2 is a regulator of both TRP channel activity and trafficking [2]. Since *cil-1* mutant males exhibit normal mating behaviors, *cil-1* appears to regulate TRPP trafficking but not activity.

In neurons, *cil-1* regulates the balance between PI species that is important for intracellular polycystin trafficking. While *cil-1* may negatively regulate polycystin insertion into the plasma membrane after initial targeting, our data are inconsistent with this model. A similar PKD-2::GFP Cil phenotype is observed in the adaptor protein 1 (AP-1) *unc-101(m1)* mutant background [14]. However, PKD-2::GFP particles are visibly moving along dendrites of both WT and *my15* (Suppl Movies 1 and 2), but not *unc-101* male sensory neurons (data not shown). Finally, PKD-2 abundance within ciliary regions is comparable between WT and *my15* (Figure 1, [16]).

Our data are most consistent with a requirement for CIL-1 in TRP-polycystin trafficking to early endosomes after endocytosis (Figure 5A, B). In RnB neurons, *cil-1* acts before STAM/HRS-mediated receptor downregulation, which transport PKD-2 and LOV-1 from early endosomes to ESCRT [15]. In CEMs, it is difficult to place *lov-1*, *cil-1*, and *stam-1* in a pathway due to additive phenotypes of double mutants. PI(3)P and PI(3,5)P2 balance in endocytic compartments is important for organelle maturation and receptor trafficking. In *cil-1(my15)*, pre-early endosomal vesicles lacking the normal destination, the PI(3)P enriched early endosomes, may simply accumulate and disperse along sensory neurons. Alternatively, *cil-1* may be required for maturation of endocytic compartments by affecting PI(3)P distribution, although this is unlikely given the normal localization of RAB-5 and STAM-1 in *my15* male sensory neurons. We propose that maintaining the balance between PI(3)P and PI(3,5)P2 by the CIL-1 5-phosphatase plays an essential role in polycystin trafficking between endocytic compartments.

Our data also reveal that *C. elegans* sperm activation is coordinated by the antagonistic actions of the CIL-1 5-phosphatase and an unidentified wortmannin sensitive target. While we cannot rule out off-target effects of wortmannin, we propose that CIL-1 and a PI3-kinase control PI(3,4,5)P3 levels. PI(3,4,5)P3 recruits and activates various effectors such as serine/threonine kinases and tyrosine kinases [30]. Cytoplasmic protein kinases and protein phosphatases are significantly overrepresented in *C. elegans* sperm [31]. Molecules such as SPE-6 serine threonine kinase [32] may regulate sperm activation downstream of CIL-1 mediated turnover of PI(3,4,5)P3.

TRPP family members play important roles in mating and fertilization of numerous species [3,7-12]. ADPKD male patients may exhibit infertility due to sperm immotility [33]. Sea urchin suREJ3 (receptor for egg jelly, a polycystin-1 homolog) and suPC2 (polycystin-2) localize to the PM proximal to acrosomal vesicles in sperm [8,34]. In mice, PKD-REJ controls postcopulatory reproductive selection via effects on sperm transport and exocytic competence during the acrosome reaction [11]. In the hermaphroditic chordate *Ciona intestinalis*, the *PKD1* homolog is expressed in testes and may act on sperm to control self-incompatibility [12]. In *Drosophila*, PKD2 may mediate sperm directional movement [9,10]. Intriguingly, mutations in the Type IV 5-phosphatase INPP5E gene cause human ciliary diseases [35,36]. According to our phylogeny tree (SF2A), *cil-1* is the closest *C. elegans* homolog of INPP5E. Further experiments are needed to determine whether CIL-1 plays an evolutionarily conserved role in TRPP complex trafficking and sperm function in other species.

Supplementary Material

Refer to Web version on PubMed Central for supplementary material.

Acknowledgments

Nancy L'Hernault provided assistance with electron microscopy. We thank Natalia Morsci, Dr. Jinghua Hu, and members of Barr laboratory, Dr. John Archibald, Ching Kung, and Andy Singson for helpful discussion, Drs. David Sherwood and Joshua Ziel for critical reading of the manuscript, Dr. Barth Grant for intestinal PI markers, Dr. Shawn X-Y. Xu for the anti-TRP-3 antibody, and Dr. Sam Ward for sharing unpublished data. Some nematode strains used in this work were provided by the *Caenorhabditis* Genetics Center, which is funded by the NIH National Center for Research Resources (NCRR), and by Dr. Shohei Mitani of the National Bioresource Project for the Nematode (Japan). This work was supported by the NIH (DK059418 and DK074746 to MMB, GM082932 to SLH), NSF (0131532 to SLH), and the PKD Foundation (to MMB).

References

1. Di Paolo G, De Camilli P. Phosphoinositides in cell regulation and membrane dynamics. Nature 2006;443:651–657. [PubMed: 17035995]
2. Nilius B, Owsianik G, Voets T. Transient receptor potential channels meet phosphoinositides. EMBO J 2008;27:2809–2816. [PubMed: 18923420]
3. Barr MM, Sternberg PW. A polycystic kidney-disease gene homologue required for male mating behaviour in *C. elegans*. Nature 1999;401:386–389. [PubMed: 10517638]
4. Barr MM, DeModena J, Braun D, Nguyen CQ, Hall DH, Sternberg PW. The *Caenorhabditis elegans* autosomal dominant polycystic kidney disease gene homologs *lov-1* and *pkd-2* act in the same pathway. Curr Biol 2001;11:1341–1346. [PubMed: 11553327]
5. Igarashi P, Somlo S. Genetics and pathogenesis of polycystic kidney disease. J Am Soc Nephrol 2002;13:2384–2398. [PubMed: 12191984]
6. Bae YK, Barr MM. Sensory roles of neuronal cilia: cilia development, morphogenesis, and function in *C. elegans*. Front Biosci 2008;13:5959–5974. [PubMed: 18508635]
7. Huang K, Diener DR, Mitchell A, Pazour GJ, Witman GB, Rosenbaum JL. Function and Dynamics of PKD2 in *Chlamydomonas*flagella. Journal of Cell Biology 2007;179

8. Neill AT, Moy GW, Vacquier VD. Polycystin-2 associates with the polycystin-1 homolog, suREJ3, and localizes to the acrosomal region of sea urchin spermatozoa. Mol Reprod Dev 2004;67:472–477. [PubMed: 14991739]
9. Gao Z, Ruden DM, Lu X. PKD2 cation channel is required for directional sperm movement and male fertility. Curr Biol 2003;13:2175–2178. [PubMed: 14680633]
10. Watnick TJ, Jin Y, Matunis E, Kernan MJ, Montell C. A flagellar polycystin-2 homolog required for male fertility in *Drosophila*. Curr Biol 2003;13:2179–2184. [PubMed: 14680634]
11. Sutton KA, Jungnickel MK, Florman HM. A polycystin-1 controls postcopulatory reproductive selection in mice. Proc Natl Acad Sci U S A 2008;105:8661–8666. [PubMed: 18562295]
12. Harada Y, Takagaki Y, Sunagawa M, Saito T, Yamada L, Taniguchi H, Shoguchi E, Sawada H. Mechanism of Self-Sterility in a Hermaphroditic Chordate. Science 2008;320:548–550. [PubMed: 18356489]
13. L'Hernault, SW. Spermatogenesis. WormBook. 2006. http://www.wormbook.org
14. Bae YK, Qin H, Knobel KM, Hu J, Rosenbaum JL, Barr MM. General and cell-type specific mechanisms target TRPP2/PKD-2 to cilia. Development 2006;133:3859–3870. [PubMed: 16943275]
15. Hu J, Wittekind SG, Barr MM. STAM and Hrs Down-Regulate Ciliary TRP Receptors. Mol Biol Cell 2007;18:3277–3289. [PubMed: 17581863]
16. Bae YK, Lyman-Gingerich J, Barr MM, Knobel KM. Identification of genes involved in the ciliary trafficking of *C. elegans* PKD-2. Dev Dyn 2008;237:2021–2029. [PubMed: 18407554]
17. Nonet ML. Visualization of synaptic specializations in live C. elegans with synaptic vesicle protein-GFP fusions. Journal of Neuroscience Methods 1999;89:33–40. [PubMed: 10476681]
18. Gurung R, Tan A, Ooms LM, McGrath MJ, Huysmans RD, Munday AD, Prescott M, Whisstock JC, Mitchell CA. Identification of a novel domain in two mammalian inositol-polyphosphate 5-phosphatases that mediates membrane ruffle localization. The inositol 5-phosphatase skip localizes to the endoplasmic reticulum and translocates to membrane ruffles following epidermal growth factor stimulation. J Biol Chem 2003;278:11376–11385. [PubMed: 12536145]
19. Bui YK, Sternberg PW. *Caenorhabditis elegans* inositol 5-phosphatase homolog negatively regulates inositol 1,4,5-triphosphate signaling in ovulation. Mol Biol Cell 2002;13:1641–1651. [PubMed: 12006659]
20. Gower NJ, Walker DS, Baylis HA. Inositol 1,4,5-trisphosphate signaling regulates mating behavior in *Caenorhabditis elegans* males. Mol Biol Cell 2005;16:3978–3986. [PubMed: 15958491]
21. Harris TW, Hartwieg E, Horvitz HR, Jorgensen EM. Mutations in synaptojanin disrupt synaptic vesicle recycling. J Cell Biol 2000;150:589–600. [PubMed: 10931870]
22. Roggo L, Bernard V, Kovacs AL, Rose AM, Savoy F, Zetka M, Wymann MP, Muller F. Membrane transport in *Caenorhabditis elegans*: an essential role for VPS34 at the nuclear membrane. Embo J 2002;21:1673–1683. [PubMed: 11927551]
23. Christoforidis S, Miaczynska M, Ashman K, Wilm M, Zhao L, Yip SC, Waterfield MD, Backer JM, Zerial M. Phosphatidylinositol-3-OH kinases are Rab5 effectors. Nat Cell Biol 1999;1:249–252. [PubMed: 10559924]
24. Okamoto H, Thomson JN. Monoclonal antibodies which distinguish certain classes of neuronal and supporting cells in the nervous tissue of the nematode *Caenorhabditis elegans*. J Neurosci 1985;5:643–653. [PubMed: 3882896]
25. Washington NL, Ward S. FER-1 regulates Ca2+ -mediated membrane fusion during C. elegans spermatogenesis. J Cell Sci 2006;119:2552–2562. [PubMed: 16735442]
26. Xu XZS, Sternberg PW. A *C. elegans* Sperm TRP Protein Required for Sperm-Egg Interactions during Fertilization. Cell 2003;114:285–297. [PubMed: 12914694]
27. Arcaro A, Wymann MP. Wortmannin is a potent phosphatidylinositol 3-kinase inhibitor: the role of phosphatidylinositol 3,4,5-trisphosphate in neutrophil responses. Biochem J 1993;296(Pt 2):297–301. [PubMed: 8257416]
28. Shi SH, Jan LY, Jan YN. Hippocampal Neuronal Polarity Specified by Spatially Localized mPar3/mPar6 and PI 3-Kinase Activity. Cell 2003;112:63–75. [PubMed: 12526794]

29. Pinal N, Goberdhan DC, Collinson L, Fujita Y, Cox IM, Wilson C, Pichaud F. Regulated and polarized PtdIns(3,4,5)P3 accumulation is essential for apical membrane morphogenesis in photoreceptor epithelial cells. Curr Biol 2006;16:140–149. [PubMed: 16431366]

30. Hawkins PT, Anderson KE, Davidson K, Stephens LR. Signalling through Class I PI3Ks in mammalian cells. Biochem Soc Trans 2006;34:647–662. [PubMed: 17052169]

31. Reinke V, Smith HE, Nance J, Wang J, Van Doren C, Begley R, Jones SJ, Davis EB, Scherer S, Ward S, Kim SK. A global profile of germline gene expression in *C. elegans*. Mol Cell 2000;6:605–616. [PubMed: 11030340]

32. Muhlrad PJ, Ward S. Spermiogenesis initiation in *Caenorhabditis elegans* involves a casein kinase 1 encoded by the *spe-6* gene. Genetics 2002;161:143–155. [PubMed: 12019230]

33. Vora N, Perrone R, Bianchi DW. Reproductive issues for adults with autosomal dominant polycystic kidney disease. Am J Kidney Dis 2008;51:307–318. [PubMed: 18215709]

34. Mengerink KJ, Moy GW, Vacquier VD. suREJ3, a polycystin-1 protein, is cleaved at the GPS domain and localizes to the acrosomal region of sea urchin sperm. J Biol Chem 2002;277:943–948. [PubMed: 11696547]

35. Bielas, SL.; Silhavy, JL.; Brancati, F.; Kisseleva, MV.; Al-Gazali, L.; Sztriha, L.; Bayoumi, RA.; Zaki, MS.; Abdel-Aleem, A.; Rosti, RO.; Kayserili, H.; Swistun, D.; Scott, LC.; Bertini, E.; Boltshauser, E.; Fazzi, E.; Travaglini, L.; Field, SJ.; Gayral, S.; Jacoby, M.; Schurmans, S.; Dallapiccola, B.; Majerus, PW.; Valente, EM.; Gleeson, JG. Nat Genet. Advanced online publication; 2009. Mutations in INPP5E, encoding inositol polyphosphate-5-phosphatase E, link phosphatidyl inositol signaling to the ciliopathies.

36. Jacoby, M.; Cox, JJ.; Gayral, S.; Hampshire, DJ.; Ayub, M.; Blockmans, M.; Pernot, E.; Kisseleva, MV.; Compere, P.; Schiffmann, SN.; Gergely, F.; Riley, JH.; Perez-Morga, D.; Woods, CG.; Schurmans, S. Nat Genet. Advanced online publication; 2009. INPP5E mutations cause primary cilium signaling defects, ciliary instability and ciliopathies in human and mouse.

37. Hu J, Bae YK, Knobel KM, Barr MM. Casein Kinase II and Calcineurin Modulate TRPP Function and Ciliary Localization. Mol Biol Cell 2006;172:663–669.

38. Fili N, Calleja V, Woscholski R, Parker PJ, Larijani B. Compartmental signal modulation: Endosomal phosphatidylinositol 3-phosphate controls endosome morphology and selective cargo sorting. Proc Natl Acad Sci U S A 2006;103:15473–15478. [PubMed: 17030795]

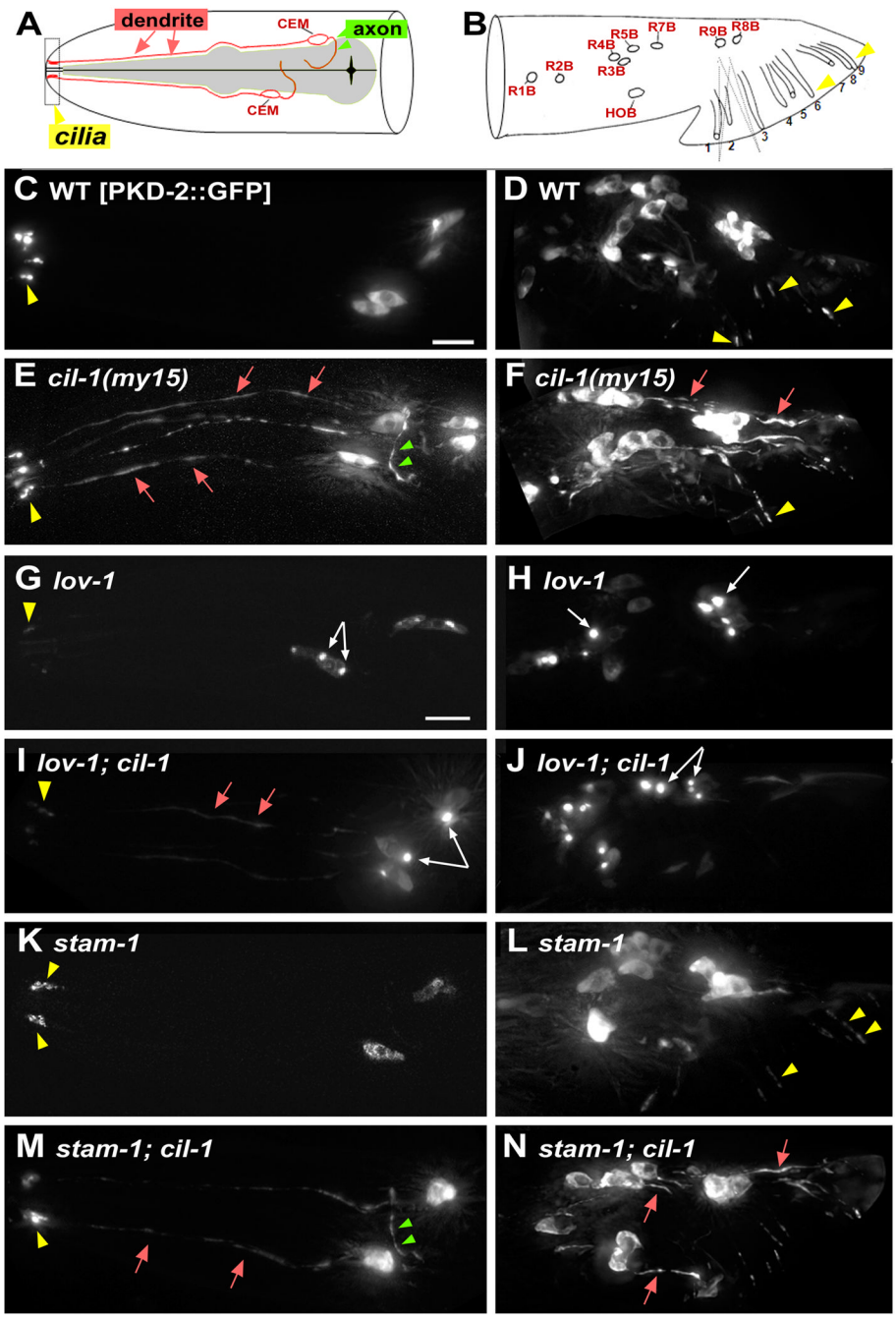

Figure 1. *cil-1* is required for TRP polycystin complex (PKD-2 and LOV-1) localization. *cil-1* acts between *lov-1* and *stam-1* in ray B neurons

Cell bodies = white arrows, cilia = yellow arrowhead, dendrite = red arrow, axon = green arrowhead. (A-B) Cartoons illustrating locations and structure of *pkd-2* expressing neurons in *C. elegans* male head (A) and tail (B). The head CEMs and tail ray neurons are bilateral, and only one side of the animal is shown. Modified from [37]. (C, D) In a WT male, PKD-2::GFP localizes to cilia and neuronal cell bodies of CEM, ray B (RnB), and hook B (HOB) neurons. (E, F) In *cil-1(my15)* males, PKD-2::GFP is abnormally distributed along neurons including dendrites and axons. PKD-2::GFP in ciliary regions appears WT. (G) In *lov-1* CEMs, PKD-2::GFP accumulates in cell bodies and weakly labels in cilia. (H) In *lov-1* RnBs,

PKD-2::GFP accumulates in cell bodies and is not detectable in cilia. (I) In *cil-1; lov-1* CEMs, PKD-2::GFP aggregates in cell bodies and distributes along dendrites and cilia. (J) In *cil-1; lov-1* RnBs, PKD-2::GFP forms bright aggregates in the cell bodies, similar to the *lov-1* single mutant. (K) In *stam-1* CEMs, PKD-2::GFP accumulates in ciliary regions. (L) In *stam-1* RnBs, PKD-2::GFP accumulates in the ciliary regions and distal dendrites [15]. (M) In *stam-1; cil-1* CEMs, PKD-2::GFP localizes to dendrites and axons, and sometimes accumulates ciliary bases. (N) In *stam-1; cil-1* RnBs, PKD-2::GFP is distributed to dendritic and axonal processes, similar to *cil-1* single mutants Scale bar, 10um.

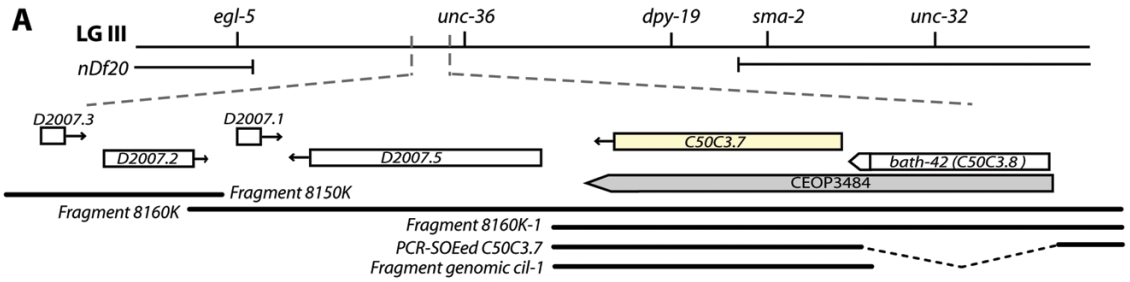

B

injected fragments	rescue? (rescing/total lines)	
	Cil	Spe (brood size)
8150K + 8160K	+ (2/2)	ND
8160K	+ (4/5)	ND
8160K-1	+ (6/6)	ND
PCR-SOEed C50C3.7	+ (2/2)	+ (2/2)
genomic cil-1	+ (1/1)	- (0/1)
Ppkd-2::cil-1(cDNA)::tdtomato	+ (3/5)	- (0/5)

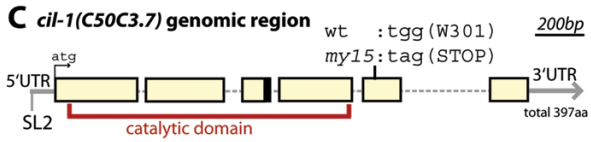

Figure 2. *cil-1/C50C3.7* encodes a phosphoinositide 5-phosphatase

(A) Genetic and physical maps of the region of LG III encompassing the *cil-1* locus. Positions of rescuing genomic fragments are aligned approximately to the physical map. (B) Summary table for rescue effects of injected *cil-1(my15)* lines. The Spe phenotype was scored by hermaphroditic brood size. (C) C50C3.7 is the gene mutated in *cil-1(my15)*. Six blank boxes indicate exons connected with five introns. *my15* is a nonsense mutation in the 5th exon (301st amino acid). The black box at the end of the 3rd exon indicates the position of alternative splicing for the short form C50C3.7b. C50C3.7a encodes a phosphoinositide 5-phosphatase and the catalytic domain is indicated in red.

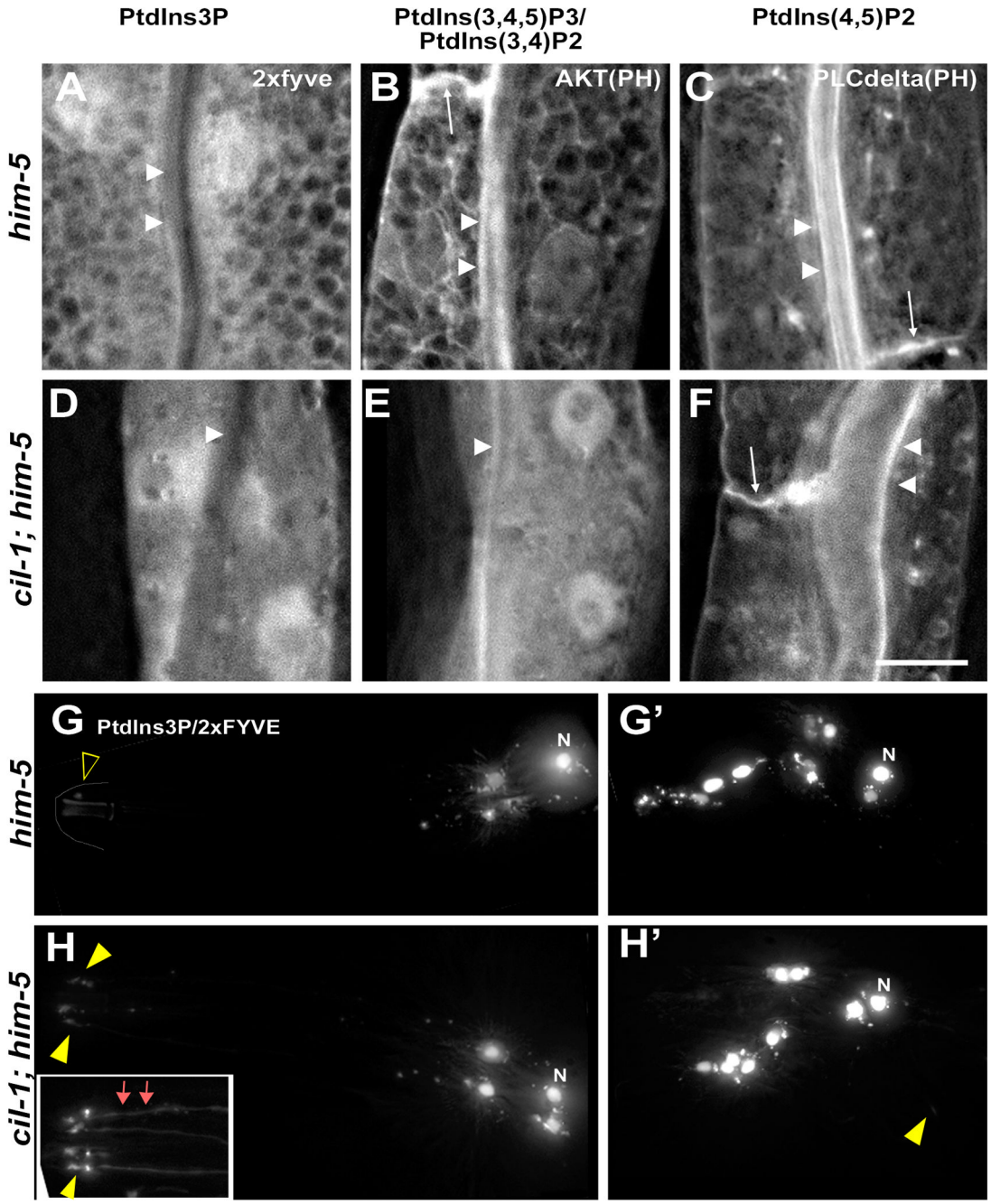

Figure 3. *cil-1* regulates PI(3,5)P2 and PI(3,4,5)P3 subcellular distribution

GFP-tagged PI specific markers in the intestine of adult males are 2×FYVE for PI(3)P, AKT (PH domain) for PI(3,4,5)P3 and PI(3,4)P2, and PLC-delta (PH domain) for PI(4,5)P2. (A-C) In the WT intestine: (A) PI(3)P labels mesh-like, tubulovesicular structures in the cytoplasm without obvious PM labeling. (B) PI(3,4,5)P3 and PI(3,4)P2 label similar tubulovesicular structures as well as the apical (arrowheads) and basolateral (arrow) PM. (C) PI(4,5)P2 predominantly labels the apical (arrowheads) in addition to the basolateral (arrow) PM. (D-F) In the *cil-1(my15)* intestine: (D) PI(3)P appears soluble in the cytoplasm. (E) PI(3,4,5)P3 and PI(3,4)P2 lose their tubulovesicular pattern, appearing diffuse in the cytoplasm. The PM labeling is less prominent in *cil-1* mutants (arrowheads). (F) PI(4,5)P2 remains enriched in the

PM. (G-H) tdTomato-tagged 2×FYVE domain (PI(3)P marker) expression in male specific neurons of WT and *cil-1(my15)*. (G) In WT CEMs, the PI(3)P marker is bright in the nuclei (denoted as N), small puncta in the cell bodies, but almost absent from cilia (blank yellow arrowhead). (G′) Similarly, in WT RnBs, the PI(3)P marker is confined to cell bodies (nuclei and small puncta). (H) In *cil-1(my15)* CEMs, the PI(3)P marker is visible in cilia and dendrites (arrows) in addition to cell bodies. The inset shows PI(3)P marker labeling ciliary and dendritic regions. (H′) In *cil-1(my15)* RnBs, the PI(3)P marker is occasionally visible in cilia (yellow arrowhead) in addition to cell bodies. Scale bar, 10um.

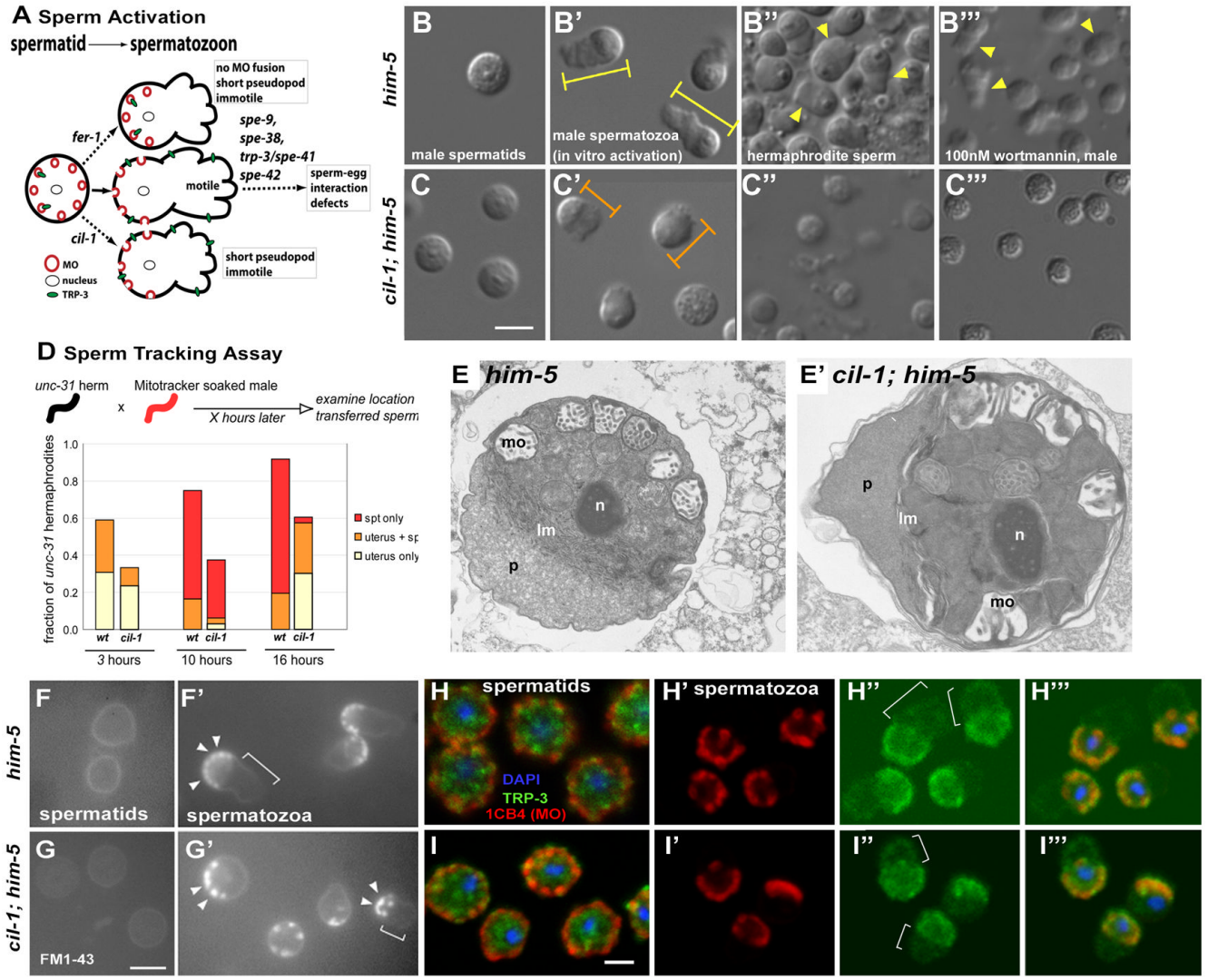

Figure 4. *cil-1* positively regulates sperm activation and motility

(A) *C. elegans* sperm activation summarized in this cartoon depicting pathways and genes functioning during sperm activation and fertilization. In a spermatid, MOs containing a TRPC receptor TRP-3 are located just below the PM. During WT activation (solid arrow), MOs fuse to the PM and a pseudopod develops, producing a motile spermatozoon. In *fer-1* mutant sperm (upper dotted arrow), MOs do not fuse with the PM and a short pseudopod forms, resulting in immotile sperm. A *cil-1* mutant sperm (lower dotted arrow) is normal in MO fusion, but develops into immotile spermatozoon with a short pseudopod. TRPC TRP-3 translocation from MO to the PM appear normal in *cil-1* mutant sperm. *spe-9*, *spe-38*, *spe-41/trp-3*, and *spe-42* encode various membrane proteins required for sperm-egg interactions. Loss of any of these genes results in motile but infertile spermatozoa. (B-C) Nomarski images of isolated male-derived sperm before and after *in vitro* activation and endogenously activated hermaphrodite-derived sperm. (B) A round WT spermatid. (B′) WT spermatozoa after 15 minute of pronase activation. Spermatozoa extend full-length pseudopods (yellow arrowheads). Yellow bars depict the length of WT spermatozoa measured. (B″) WT hermaphrodite-derived sperm that are endogenously activated. (B‴) WT male-derived sperm are activated to spermatozoa with pseudopods (arrow arrowheads) within 10 minutes upon 100nM wortmannin application. (C)

cil-1(my15) mutant spermatids before activation are slightly smaller than WT spermatids. (C′) Upon activation, *cil-1* mutant sperm develop stubby pseudopods. The length of sperm is indicated with orange bars shorter than WT (compare to yellow bars). (C″) Hermaphrodite-derived sperm from *cil-1(my15)* mutant occasionally develop short pseudopods. (C‴) *my15* male-derived sperm are not activated by 100nM wortmannin but exhibit subtle morphological changes. (D) Sperm Tracking Assay. The majority of WT male-derived sperm are deposited and retained within the spermatheca in the hermaphroditic reproductive tract at 10 and 16 hours. In contrast, *cil-1(my15)* male-derived sperm are not found in the spermatheca at 16 hours. (E-E′) Ultrastructure of *him-5(e1490)* (E) and *cil-1(my15) him-5(e1490)* (E′) spontaneously activated spermatozoa.

Abbreviations: lm, laminar membranes; mo, membranous organelles; n, nucleus; p, pseudopod. While the cytoplasm in this *cil-1* pseudopod (compare E to E′) appears denser than that of the WT control, the significance, if any, of this observation is unclear. (F-G) Monitoring MO fusion during sperm activation with a lipophilic FM1-43 dye. (F) The PM of WT spermatids is stained with FM1-43. (F′) In WT spermatozoa, the dye concentrates at the MO fusion sites. MO fusion events are restricted to the PM of cell body (arrowheads) but not pseudopod (bracket). (G) FM1-43 dye marks the PM of *cil-1* spermatids. (G′) In short *my15* spermatozoa with visible pseudopods, MO fusion sites are concentrated on the cell body (arrowheads) and excluded from the pseudopod PM (bracket). (H-I) Immunohistochemistry of sperm using the MO antibody 1CB4 (red), anti-TRP-3 (green), and DAPI (blue). The triple labeled image were generated by overlaying three confocal images from the same Z-section. (H) In WT spermatids, MOs (red) are located around the cell periphery below the PM. Location of TRP-3 (green) partially overlaps with 1CB4 labeled MOs. (H′) In WT spermatozoa, 1CB4 positive MOs are primarily located around the PM, but absent from pseudopods (compare with bracket area in H″). (H″) In WT spermatozoa, anti-TRP-3 staining is detectable in the cell body and pseudopod PM (bracket). (H‴) Overlay of WT spermatozoa. (I) In *my15* spermtids, MOs (red) are localized to the cell periphery just below the PM as in WT. Anti-TRP-3 staining (green) overlaps with MOs. (I′) In *my15* spermatozoa, similarly to WT, MOs are found in the cell body but not pseudopod. (I″) In *my15* spermatozoa, TRP-3 protein is detected both in the cell body and pseudopod, as in WT. (I‴) Overlay of H′ and H″ with the DAPI image. Scale bar, 5um

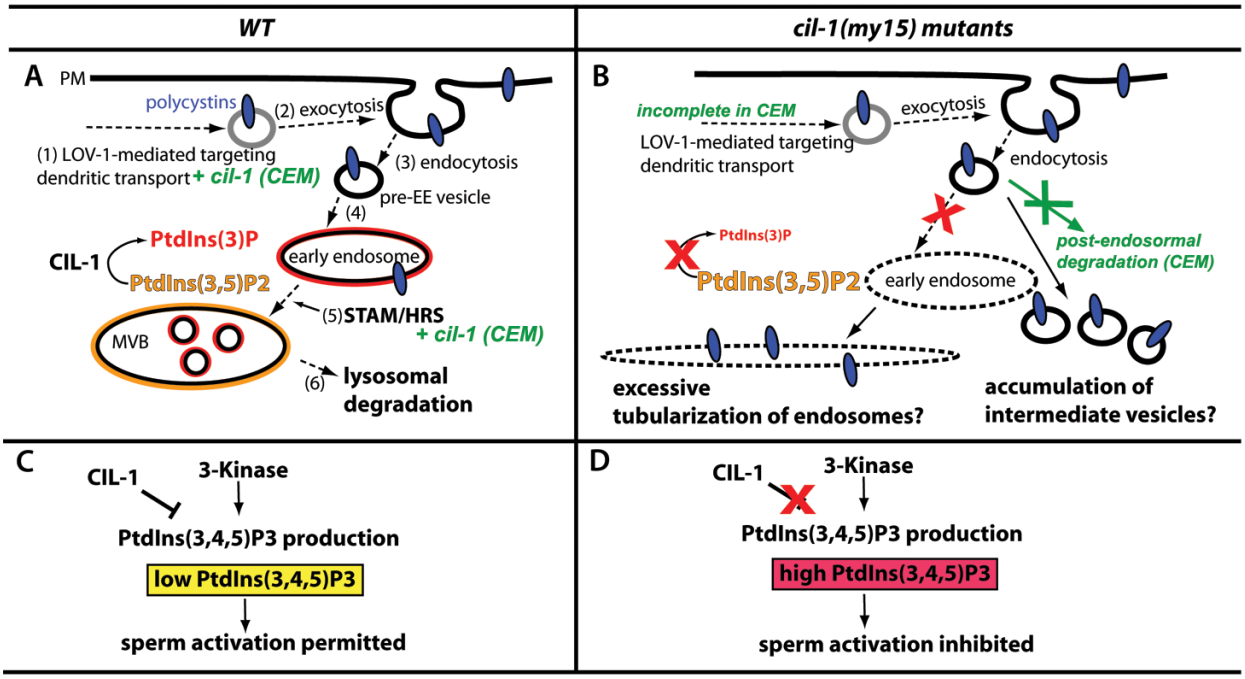

Figure 5. Models of CIL-1 functions

(A-B) A model for CIL-1 function in polycystin trafficking in sensory neurons. (A) In WT RnB neurons, polycystins are (1) assembled in the cell body, transported along the dendrite, and (2) exocytosed at the PM, presumably at the ciliary base. Ciliary abundance of polycystins is tightly regulated by dynamic (3) internalization/endocytosis. (4) Pre-early endosomal (pre-EE) vesicles are sorted to PI(3)P enriched (red lining) EE, followed by (5) targeting to MVB. CIL-1 functions to maintain the balance between PI(3)P and PI(3,5)P2 in the EE and MVB membrane. Polycystin sorting from EE to MVB requires the STAM/HRS complex. (6) Lysosomal degradation downregulates the polycystins. In CEM neurons, *cil-1* act at least partially in parallel with *lov-1* and *stam-1*, as indicated with green. (B) In *cil-1(my15)*, the Cil defect may occur after endocytosis. Loss of CIL-1 function causes depletion of PI(3)P, which in turn affects EE biogenesis and maturation. As shown in [38], pre-EE vesicles form an excessively tubularized EE along the microtubule network. Alternatively, polycystin-containing pre-EE vesicles may accumulate in neurons as their destination point (PI(3)P enriched EE) is blocked. In *my15* CEM neurons, loss of *cil-1* affects dendritic targeting and post-endosomal degradation (in green). (C-D) A Model for CIL-1 function in sperm activation. (C) In a WT spermatozoon, lowering PI(3,4,5)P3 (yellow) by CIL-1 action initiates unidentified signaling pathway(s) to coordinate pseudopod extension and sperm movement. An unidentified 3-kinase that generates PI(3,4,5)P3 negatively regulates sperm activation. The balanced action between CIL-1 and 3-kinase maintain low levels of PI(3,4,5)P3, permitting sperm activation. (D) In *cil-1* mutant sperm, abnormally high PI(3,4,5)P3 levels inhibit downstream signaling pathways for pseudopod extension and sperm motility.